Kinetic rate constants of gold nanoparticles deposition on silicon

*Valentina Onesto[1], Francesco Gentile[2], Mario Russo[1], Marco Villani[3], Patrizio Candeloro[1], Gerardo Perozziello[1], Natalia Malara[1], Enzo Di Fabrizio[4], M Laura Coluccio[1]**

[1] Department of Experimental and Clinical Medicine. University Magna Graecia, Catanzaro, 88100, Italy

[2] Department of Electrical Engineering and Information Technology, University Federico II, 80125, Naples, Italy

[3] IMEM-CNR, Parco Area delle Scienze, 37/A 43123 Parma, Italy

[4] Physical Science & Engineering Division, King Abdullah University of Science and Technology, Thuwal, 23955-6900, Saudi Arabia

KEYWORDS. gold nanoparticles, kinetic constants, UV-Vis spectra, electroless metal deposition, SEM analysis, porous silicon microparticles

ABSTRACT. We fabricated gold nanoparticles on nanoporous silicon microparticles using electroless deposition in a hydrofluoric acid solution containing gold chloride. The reaction was followed by UV spectrometer analysis of the absorbance of the solution (proportional to the nanoparticles concentration) for two temperatures (20°C and 50°C). Results indicate that the process is autocatalytic, described by a pseudo-first order reaction, the apparent rate constant k_{obs} of which was determined utilizing UV spectrometer data. We found that the reaction rate constant at 20°C is $7 \cdot 10^{-3}$ s^{-1}, and at 50°C is $2.9 \cdot 10^{-2}$ s^{-1}. Scanning electron microscope (SEM) analysis of samples and diffusion limited aggregation (DLA) simulations were used to validate

results. This study aims to resolve the kinetics of electroless deposition of gold on silicon at the nanoscale, in the present state of art missing a quantitative characterization, for certain conditions of growth and given values of temperature and concentration of the reagents. Results may have applications to the synthesis of gold nanoparticles, and their use as nanosensors, drug delivery systems, or metal nano- meta- materials with advanced optical properties.

INTRODUCTION

Metal nano materials are of interest for those working in research and industry, owing to their improved physical and chemical characteristics and potential impact in fields such as electronics, medicine, biomedical engineering. The shape and the size of nanoparticles together with their organization in micro/nano structures influence their electrical and optical properties, increasing the attention in metal nanoparticles realization methods [1]. The controlled synthesis of metal nanoparticles or the deposition of a metallic layer is a challenge for nanotechnology research to improve the possibility of creating well-defined nanostructures exhibiting those physical and chemical characteristics required by specific applications.

Techniques for the synthesis of metal nanoparticles range from chemical methods, prevalently consisting in redox reaction or electroless processes [2, 3], , to electrochemical deposition [4], electron beam evaporation [5], chemical vapor deposition [6], or chemical spray pyrolysis [7]. In all cases, the aim of technique is granting maximum control over the size and shape of the final metal nanostructures. Two different strategies are being currently pursued to achieve a similar target, being:

(i) a combination of nanotechnology and chemical techniques, where the former (including optical lithography, electron beam lithography, focused ion beam) create defined patterns where particles are deposited – typically by a chemical reaction of reduction; or,

(ii) pure chemical methods, where an accurate choice and tuning of the process parameters (reactants concentrations, temperature, presence of additives, to cite a few) yield final structures with the intended characteristics.

In both cases, electroless deposition is a key step of the process. Electroless deposition is a controlled autocatalytic deposition of metals on a surface by the reaction of a complex compound and a chemical reducing agent. It has recently attracted attention for its potential use in electronics, bioelectronics, biomedicine, energy, because of its ease of use, cost-effectiveness, tight control on shape and size of the intended structures, high precision and reproducibility.

Electroless deposition involves the nucleation and growth of metal nanoparticles starting from the reduction in aqueous solutions of precursor metal salts by means of a reducing agent [8]. In a very commonly used version of this technique, the reducing agent is a substrate of silicon (Si): metal reacts oxidizing Si and reducing itself to metallic nanoparticles [3]. The optical properties of silver and gold nanoparticles make them largely used metals for fabrication of nanostructures with plasmonic behavior [9, 10]. In previous reported works, we have used a similar process to obtain nano-porous silicon substrates decorated with gold nanoparticles for cell-surface SERS analysis [11, 12], and plasmonic devices with arrays of ordered silver nano-particles for single molecule detection and biodetection [3, 9].

The output of the process and the characteristics of the structures exhibit a great very sensitivity to the parameters of the process, including temperature, concentration, reagents characteristics. To attain the maximum control over the technique and optimizing performance, one has to know the kinetics parameters of the reaction of electroless deposition. Several reports in literature investigated this process, sometimes focusing on specific reactions, especially pertaining the growth of gold or silver nanoparticles.

In reference [13], Esumi et al. study the kinetic of gold and silver nanoparticles formation in aqueous solution of sugar-persubstituted poly(amidoamine) dendrimers in reference [14], Ismail

et al study by reduction of silver(I) in the presence of surfactants and macromolecules, Patakfalvi and colleagues investigated the kinetics of homogeneous nucleation of silver nanoparticles stabilized by polymers [15]. The mechanism of the reaction of gold chloride and the associated kinetics parameters were found for the special cases of reaction with formic acid [16], and reaction with silicate surfaces [17]. Nevertheless, at the best of our knowledge, no studies report the electroless rate kinetics of deposition of gold on silicon surface.

Here, we examined the reaction of gold chloride ($AuCl_3$) with nanoporous silicon to determine its kinetics characteristics. We used for the study porous silicon nanoparticles (PSNPs), prepared by silicon anodization in an electrolytic cell containing a solution of fluorhydric acid (HF/water/ethanol), followed by ultrasonication of the silicon substrate [11]. Gold nanoparticles were realized adding to a solution of $AuCl_3$ an appropriate amount of PSNPs (**Figure 1**). We then replicated the experiment setting two different values of temperature, $T_1 = 25°$ and $T_2 = 50°$ (Methods). Since the optical properties of gold colloidal solutions depend on the particle size and density [18], we monitored these variables over time deriving them from the light absorbed from the particles in solution as described in the methods.

It is known that particles with a characteristics size below the wavelength of visible light generate, in response to an external electromagnetic radiation, either absorption or scattering phenomena [19]. One and the other are more or less relevant in relation to the particle size and the characteristics of the dielectric medium. For metals as silver or gold, the excitation of plasmon resonances in small particles (with a size less than approximately $70\ nm$ for gold) lead mainly to absorption of light. On the contrary, when particle size approaches the wavelength of visible light ($> 350\ nm$), scattering offers the major contribution [20]. For the present configuration, SEM inspection of samples reveals that the mean particle size is mostly below λ –

approaching 200 nm *only* at high temperatures ($T_2 = 50°C$) and long reaction times ($t > 60\ min$) (**Figure 2**).

On this basis we have assumed scattering less relevant than absorption: taking the latter, measured by an UV spectrometer, as an indicator of characteristics of the systems and the principal parameter from which to derive the time evolution of the system and its kinetics constants.

MATERIALS AND METHODS

Fabrication of porous silicon nanoparticles. Nano-porous silicon nanoparticles were obtained from nano-porous silicon substrates by ultrasonication. The procedure to realize a network of nano-pores in silicon flat samples consists on the anodization of boron-doped silicon wafer (100) with resistivity 5–10 Ω-cm, using an electrolyte mixture of hydrofluoric acid (25%), water (25%), and ethanol (50%). A current density cell of 20 mA/cm^2 was applied to the electrolytic cell for 5 min at 25 °C. Samples were then rinsed by series washes in deionized water, ethanol and pentane [17, 21-23].

Electroless deposition of metals on silicon nanoparticles. In electroless deposition, metal ions in solution react with a reducing agent and the product metal nanoparticles are deposited on a substrate. The general law of the electroless process is:

$$Me^{n+} + Red = Me^0 + Ox \qquad (1)$$

where Me^{n+} are metal ions and Red is the reducing agent. n electrons are exchanged between Red and metal ions to produce the atomic metal Me^0. When the substrate is silicon, metal reduction is catalyzed by silicon, which contemporary reacts as reducing agent, yields electrons to the metal ions.

In the case of gold ions in solution, the reaction takes the form:

$$Si + 2H_2O = SiO_2 + 4H^+ + 4e^- \qquad (2)$$

silicon oxidation occurring at the anode, and

$$Au^{3+} + 3e^- = Au^0 \qquad (3)$$

gold reduction at the cathode [24]. Particle growth takes place by an initial nucleation phase with the formation of metallic nuclei, followed by a step of growth. Temperature, time of reaction and type of metals and the concentration of the solution's components, influence the driving force of the reaction, the potential difference between the products and the reagents, as the shape and size of the growing nanoparticles. Here we have used a base solution of Hydrofluoric acid 0.15M and gold chloride ($AuCl_3$) 5mM. De-ionized (D.I.) water (Milli-Q Direct 3, Millipore) was used for all experiments. Gold chloride ($AuCl_3$) was purchased from Sigma and Hydrofluoric acid (HF) 50% RPE ACS-ISO from Carlo Erba Reagents. All chemicals, unless mentioned otherwise, were of analytical grade and were used as received. P-type (100) silicon wafers were used as substrates. Substrates were cleaned with acetone and ethanol to remove possible contaminants. Hydrofluoric acid in solution has the function to eliminate the superficial oxide and create the dangling bonds necessary for metal reduction, as in the following reaction:

$$SiO_2 + 6HF = {SiF_6}^{2-} + 2H^+ + 2H_2O. \qquad (4)$$

Kinetics procedure. A test tube containing 10 ml of $AuCl_3$ - HF solution was thermally equilibrated at the desired temperature (T1 environmental temperature, T2 50°C) in a constant temperature water bath. The reaction was started by adding 50 µl of PSNPs into the acid solution. The progress of the gold nanoparticles formation was followed spectrophotometrically by measuring the absorbance against blanks at definite time intervals at a wavelength of 560 nm, corresponding to the max peak in the absorption spectrum of the gold nanoparticles/HF solution (**Figure 3**). The UV–visible spectra of the samples were recorded for the wavelength range 300–

900 nm at 2-min intervals on a Perkin-Helmer Lambda spectrophotometer. The apparent rate constant k of the gold/silicon reaction was determined from the slope of the plot $\ln(a/1-a)$ vs time, where $a = A_t/A_\infty$; A_t is the maxima absorbance at time t and A_∞ is the absorbance at ∞ [11].

Scanning Electron Microscopy analysis of samples. A Field Emission Gun - Scanning Electron Microscope (FEG-SEM) Zeiss Auriga equipped with high efficiency annular secondary detector (in lens) was used to evaluate the morphology of Au NP deposited on silicon. Accelerating voltage was set at 15 kV.

Image analysis of SEM micrographs. SEM images were analysed with Matlab® to extract nanoparticles diameter. Images were first converted to grayscale, preprocessed to enhance contrast by contrast-limited adaptive histogram equalization (CLAHE) and low-pass filtered to remove constant power additive noise before being binarized with Otsu's method. Morphological opening was performed to remove any small white noises in the image, and morphological closing to remove any small holes in the object. All connected components that had fewer than 20 pixels were removed and structures that were connected to the image border were suppressed. The images were segmented by a watershed transformation and a distance transform was used as segmentation function to split out the regions. With watershed segmentation, single nanoparticles were identified. The corresponding diameters were extracted through the regionprops function.

RESULTS AND DISCUSSION

Experimental analysis of gold nanoparticles growth and kinetics. Results, **Figure 3,** are represented graphically as absorbance-wavelength profiles for two temperatures T1 and T2, corresponding to 20°C and 50°C respectively. The absorbance is dimensionless, it is not expressed as a fraction or a percentage: with Lambert-Beer the absorbance is defined as $A =$

$\log_{10}(I_0/I)$, where I_0 is the intensity of the initial incident radiation, and I is the intensity of the radiation after leaving the medium. Since the transmittance is defined as $T = I/I_0$, one can express A in terms of T as: $A = log_{10}(1/T)$. This automatically implies that, for any T<0.1 (i.e. the transmittance is lower than 10% of the initial radiation) A>1, thus values of absorbance greater than one are admissible, coherently with some of the results presented in Figure 3. The absorbance profile for both temperatures is typical of a solution containing gold nanoparticles: just after mixing the two solutions ($HF/AuCl_3$ and PSNPs in water), the recorded UV–visible spectra of the mixture shows a maximum, a hump, around 560 nm, corresponding to the formation of the gold nanoparticles, which, in fact, manifest a maximum of UV absorbance around 520-560 nm [19, 20]. Increasing the reaction time, it is observable an increase of the maximum absorbance at about 560 nm, in particular for the reaction occurring at 50°C. This indicates the proceeding of the reaction with new gold nanoparticles formation. The higher is the temperature, more are the metal ions reduced and higher is the concentration of gold nanoparticles.

The reaction kinetic is deduced observing the evolution of absorption at 560 nm with time (**Figure 4**). The starting of the reaction for both temperatures is slowly, followed by a rapid increase in Abs, more evident for the reaction at 50°C. In this last case, we note an induction time from the start of the reaction to about 20 min, a step between 20 min and about 120 min in which reaction proceeds very quickly, and a final step in which Abs tends to a plateau due to residual reaction, around 300 min. When temperature is 20°C the three steps are less evident and each phase is longer: the induction time is in the range 0-30 min, the second step, core of the reaction, occurs in the range 30-240 min, and the third stage over 240 min, suggesting an obvious slower reaction respect to the hot process.

In **Figure 4** data are fitted with sigmoidal curves (red lines), characterized by an initial slow stage indicating an induction period, a second stage manifesting a more or less rapid increment in gold nanoparticles concentration and a final steady state stage. The behaviour of the

$Au/PSNPs$ system, therefore, leads to think that an autocatalytic process is occurring, during which the second stage is a central period of auto-acceleration. In autocatalysis, a reaction product is a reactant and at the same time a catalyst for the same or a combined reaction. At the first metal ions in solution react with silicon microparticles reducing themselves and oxidizing silicon. In a second step, the newly made gold nanograins facilitate the electrons exchange between silicon and gold ions, accelerating the reaction, and so acting as catalysts, as described by equations 4.

$$(Me^0)_n + Me^{n+} = (Me^0)_{n+1} \qquad (4)$$

Results obtained by UV spectrometry lead to thinking to a mechanism of gold nanoparticles synthesis near to the method proposed by Turkevich [25] and later studied by J. Polte [26] precisely on gold nanoparticles synthesis. The method divides the growth mechanism in four steps: 1) rapid reduction of the gold precursor and nucleation; 2) coalescence of the nuclei and formation of nanoparticles; 3) diffusional growth step and 4) autocatalytic surface reduction. The first two steps are decisive to determine the total number of nanoparticles that will be formed, while in the last two steps the gold ions in solution are reduced on the present particles and, in particular, the process becomes very fast during the autocatalytic surface reduction. In the present study, the first three steps can be grouped in the induction period, instead the fourth steps can be attributed to the central period of auto-acceleration, prominent in the reaction, driving us to center on it the kinetic investigation. This choice permits us also to neglect porosity effect of the nanoparticles. In fact, if generally porosity influences kinetic of the reaction changing the contact area and the diffusion of reactants in the porous material, in the reaction between NPSi and Au ions, porosity weights only in the first stage (induction time) when the gold nanoparticles are immediately formed after the contact between silicon and gold ions and have still dimensions comparable with pores' size and so diffusion into the porous material of products and reagents is still possible. Instead, during the second stage, for which we have calculated K_{obs}, gold

nanoparticles grow on the surface of the silicon nanoparticles and their sizes are greater than pores dimensions, suggesting that reaction, at this stage, occurs only on a surface level. Considering the characteristic of an autocatalytic process of the $NPSi/AuCl_3$ reaction, we follow the progress of reduction by the function $\ln(a/1-a)$, which is expected to have a linear trend against the reaction time, as it happens in simple autocatalysis [9, 10, 27]. The linear behavior in the intervals of time comprehending the induction and the reaction phases is confirmed by the plots of ln(a/(1-a)) versus time (**Figure 5**). Consequently, a pseudo first-order kinetic with respect to gold ions Au^{3+}, in excess of silicon nanoparticles concentration, is an acceptable assumption. The rate law is, therefore, represented by $\frac{d[Au^{3+}]}{dt} = k_{obs}[Au^{3+}]$ where k_{obs} depends from temperature.

The observed rate constants (k_{obs}) are determined from the slopes of the linear fit to the plots in the range 0-120 min: the rate constant at 20°C is $7 \cdot 10^{-3}$ s^{-1}, while the rate constant at 50°C is $2.9 \cdot 10^{-2}$ s^{-1}. (**Table 1**)

Observing graphs of Abs vs wavelength (**Figure 3**), it is perceptible that the absorption band, at 560 nm, due to the presence of the gold nanoparticles, undergo a minor shift from 560 to 540 nm, as evident in **Figure 6** where the absorption band value is reported vs time. When the electroless reaction occurs at around 20°C, the shift of the maximum absorption band wavelength with time progression appears as a linear trend in the range 0-120 min, with a slope of -0.11 and a final wavelength value of the maximum absorption band of 547 nm, other that it remains around constant. When reaction temperature is 50°C, the variation in the maximum absorbance band wavelength is faster and a linear trend can be used to fit the first 50 min, obtaining a slope of -0.44, then a gradient 4 times higher than at 20°C. The tendency of the same peak at 50°C, after 50 min is near an asymptotic value around 542 nm.

It is known, as Mie's theory [28], that optical properties, such as absorption maxima and absorption intensity, are particle size dependent [18]. In our measurements, the decreasing with

time of the maximum absorption band for both tested temperatures, indicates a diminution of the gold particles' diameter. Solutions get richer of nanoparticles, the absorption values increase, but, at the same time, size of the new formed nanoparticles decreases. During this period ($30-120$ min for T1 and $20-50$ min for T2) reaction is in the auocatalytic phase, and clustering of nanoparticles contemporary occurs, promoting the formation of nanoparticles with diameters higher than 200 nm, as observable by SEM images (**Figure 1,7**). These larger particles fall and deposit at the bottom of solution, consequently their contribute is not observable in a scattering peak at higher frequencies [29]. In solution only the smaller gold nanoparticles remain, with an increment of Abs, which justifies the increment of their density, but a diminution of wavelength of the maximum absorption peak, corresponding to the decreasing of their size [9]. The final diameter depends on the concentration of metal ions but also on colloidal stability, as most of discussed synthetic models regarding nanoparticles growth [26].

SEM images (**Figure 1, 7**) of nanoparticles at different time, for both temperatures, confirms that greater gold nanoparticles clusters are present at advanced reaction times, but contemporary the existence of small nanoparticles is manifest. In **Figure 7** two steps points are reported for each temperature in order to understand the time evolution of the reaction. Consequently, the time points steps were for T1 10 min and 120 min and for T2 10 min and 60 min, corresponding to the intervals in which the reaction is of pseudo first order. Overcoming these limits, reaction slows down and particles sizes remains almost constant, around 350-400 nm.

A comparison of SEM images taken using different modalities of detection (NTS BSD and In Lens) enables to derive the efficiency of the electroless deposition, as described in Supporting Information. The efficiency of deposition is greater than 80% for all configuration of growth and approaches unity in all cases for deposition time greater than approximately 40 min.

DLA simulations. We used a diffusion limited aggregation (DLA) scheme, precedently described in reference [23], to simulate the gold nanoparticle growth around spherical nano-

porous silicon precursors. In the simulations, the initial line of nucleation sites is a circle, representing the nano-porous silicon particle, with variable radius. We then use cellular automata to reproduce the displacement of gold ions in the domain prior deposition, with the underlying assumption that the trajectory of gold ions is random. Upon contact with the circular seed, ions in the grid are incorporated by the seed: an aggregate of a great many of smaller constituents is then formed by iteration (**Figure 8a**). For the present configuration, the sticking probability p of an ion to the aggregate is set as $p = 1$. Deterministic adhesion indicates that chemical reactions at the interface dominate over diffusion, the diffusion time being vastly larger than the deposition time. **Figure 8a** reports the steady state shape of the aggregates after 1 M cycles for the initial radius of curvature R of the seed varying between $R = 10$ and $R = 40$ pixels. For all reported values of R, the aggregate has a dendritic structure, with a succession of symmetric/non-symmetric branchings creating a nested tree, similar to fractals. The time evolution of the total mass of the aggregates is reported in **Figure 8b** for a radius of curvature $R = 30$ pixels - the diagram reproduces the total mass N of the aggregate at a specific time t. At the early time of the process, the kinetics of formation of the aggregates is fast, with an initial bust in correspondence of which particle growth occurs instantaneously. After an initial expansion, gold nanoparticles continue to growth at a constant rate, consistently with the experimental results reported in **Figures 4** and **5**. The out-put of the model matches with the measured particle growth with a good level of accuracy at the initial time of the process. However, the DLA model does not reproduce the constant, steady-state regime as in the experiments, possibly because in the model ions are constantly released in the system (DLA model with constant source), while in real experiments the amount of gold chloride in solution is finite, and after consumption of the ions in solution the process cannot proceed indefinitely. In **Figure 8c** we report the curves of growth for all considered radius of curvature at the interface between the nano-porous silicon particle deposition layer and the solution: $R = 10, 20, 30, 40$ pixels. The rate of deposition and the overall aggregate mass deposited over time steadily increases with R, that is easily explained

considering that the larger R, the higher the surface with which ions can interact. Nevertheless, and quite remarkably, the picture changes when one considers the density in place of the total mass of the aggregate. We define density of an aggregate, ρ, the value of its mass to the circumference of the initial seed upon which the aggregate was formed: $\rho = N/2\pi R$. In **Figure 8d** ρ is reported as a function of time for different values of R. The density rises more steeply for the smallest $R = 10$, while the kinetics of growth is hampered for higher values of R. These findings are reinforced by the diagram in **Figure 8e**, where ρ, measured at the steady state, has a maximum at $R = 10$ and a minimum at $R = 30$ pixels. Results suggest that the process of chemical deposition – globally – takes advantage from a small size of the initial nucleation site. The morphological characteristics of the aggregates were investigated using the methods reported in reference [23]. For each configuration, we derived the density-density correlation function $c(r)$ associated to the aggregate: $c(r)$ contains the information about the internal architecture of a system as a function of system size r. We observe that the aggregates exhibit a scaling law behavior typical of fractals (**Figure 8f**). From the slope of β of $c(r)$ in a log-log plot, we derived the corresponding value of fractal dimension as $D_f = 2 - \beta \sim 1.667$, close to the theoretical limit $5/3$.

Regarding simulation's results, it is to note that we modelled the process of particle growth in a 2D space for mathematical convenience and to assuring fast computation times. While the process of electroless growth is 3-dimensional, this simulations campaign was not focused on reproducing the real growth and was more focused on finding a qualitative correlation between the particle radius of curvature (R) and the efficiency of growth, expressed in terms of the normalized density ρ. The aim of the simulations was establishing whether ρ was a function of R, i.e., whether the particle radius may influence the growth of gold on its external shell. Results indicate that ρ heavily depends on R. More sophisticated 3D numerical models that will be developed over time, may indicate that a similar dependence is even more relevant than in simplified 2D schemes. In 3D geometries, the surface exposed to electroless growth increases

with the square of the particle radius ($S \propto R^2$), differently from the 2D analogue, where the border of the particle exposed to growth varies linearly with R, $S \propto R$.

CONCLUSIONS

Gold nanoparticles were prepared on silicon microparticles by an electroless autocatalytic method. The reaction follows a pseudo first order kinetic and the observed kinetic constant is valuable measuring the absorbance of the solution by means of UV-visible spectrometer and calculating the slope of the plot $\ln(a/1-a)$ vs time ($a = A_t/A_\infty$; A_t is the maxima absorbance at time t and A_∞ is the absorbance at ∞). Results (trend on absorption peak of gold and SEM analysis) evidence that when reactions are completed, the maximum diameter of the gold particles is around 294 nm at $20°C$ and 650 nm at $50°C$ and also the concentration of nanoparticles, related to the absorbance of the reaction solution, is higher for the highest temperature. Then, spectroscopic analyses, calculation of the kinetic constant, SEM observations and size distributions show that reaction rate increases with temperature, as expected, but at the same time, higher temperatures generate an increment of the medium nanoparticles sizes and of the gold nanoparticles density.

ASSOCIATED CONTENT

Supporting Information. The SUPPORTING INFORMATION.pdf file report the efficiency of the electroless deposition valuated by the comparison of SEM images.

AUTHOR INFORMATION

Corresponding Author

*email: coluccio@unicz.it

Author Contributions

Conceptualization, M.L.C and F.G.; Methodology, M.L.C.; experiments and UV analyses M.R .and O.V., DLA Simulation, O.V. and F.G.; Validation, P.C., M.V., N.M. and G.P.; SEM Analysis, M.V.; Resources, E.D.F.; Writing – Original Draft Preparation, M.L.C., N.M. and F.G.; Supervision, M.L.C., F.G. and E.D.F..

Funding sources. This work was supported by the project for Young researchers financed from the Italian Ministry of Health "High Throughput analysis of cancer cells for therapy evaluation by microfluidic platforms integrating plasmonic nanodevices" (CUP J65C13001350001, project No. GR-2010-2311677) granted to the nanotechnology laboratory of the Department of Experimental and Clinical Medicine of the University "Magna Graecia" of Catanzaro

Conflicts of Interest. The authors declare no conflict of interest

REFERENCES

(1) Desai R., Mankad V., Gupta S. K, and Jha P. K. Size Distribution of Silver Nanoparticles: UV-Visible Spectroscopic Assessment. *Nanosci Nanotechnol Lett* **2012**, *4* (1) 30-34.

(2) Sosnin I.M., Turkov M.N., Shafeev M.R., Shulga E.V., Kink I., Vikarchuk A.A., Romanov A.E. Synthesis of silver nanochains with a chemical method. *Mater Phys Mech* **2017**, *32*, 198-206.

(3) Coluccio M.L., Das G., Mecarini F., Gentile F., Pujia A., Bava L., Tallerico R., Candeloro P., Liberale C., De Angelis F., Di Fabrizio E. Silver-based surface enhanced

Raman scattering (SERS) substrate fabrication using nanolithography and site selective electroless deposition, *Microel Eng* **2009**, *86* (4–6) 1085-1088.

(4) Wei C., Wu G., Yang S. & Liu Q. Electrochemical deposition of layered copper thin films based on the diffusion limited aggregation. *Sci Rep* **2016**, *6*, 34779;

(5) Shamala, K.S., Murthy, L.C.S. & Narasimha Rao, K. Studies on tin oxide films prepared by electron beam evaporation and spray pyrolysis methods, *Bull Mater Sci* **2004**, *27*, 295.

(6) Crowell J. E., Chemical methods of thin film deposition: Chemical vapor deposition, atomic layer deposition, and related technologies *J Vac Sci Tech A* **2003,** *21*, S88.

(7) Ayouchi R., Martin F., Leinen D., Ramos-Barrado J.R., Growth of pure ZnO thin films prepared by chemical spray pyrolysis on silicon. *J Cryst Growth* **2003**, *147* (3-4) 497-504.

(8) Goia Dan V. and Matijevic E. Preparation of monodispersed metal particles, *New J Chem* **1998**, 120-1215.

(9) Coluccio M. L., Gentile F., Das G., Nicastri A., Perri A.M., Candeloro P., Perozziello G., Proietti Zaccaria R., Totero Gongora J.S., Alrasheed S., Fratalocchi A., Limongi T., Cuda G., Di Fabrizio E. Detection of single amino acid mutation in human breast cancer by disordered plasmonic self-similar chain. *Sci Adv* **2015**, *1*(8).

(10) Jahn M., Patze S., , Hidi I.J., Knipper R., Radu A. I., Mühlig A., Yüksel S., Peksa V., Weber K., Mayerhöfer T., Cialla-May D. and Popp J., Plasmonic nanostructures for surface enhanced spectroscopic methods. *Analyst* **2016**, *141*, 756-793.

(11) Coluccio M.L., De Vitis S., Strumbo G., Candeloro P., Perozziello G., Di Fabrizio E., Gentile F. Inclusion of gold nanoparticles in meso-porous silicon for the SERS analysis of cell adhesion on nano-structured surfaces. *Microelectron Eng* **2016,** *158*, 102–106.

(12) Gentile F., La Rocca R., Marinaro G., Nicastri A., Toma A., et al. Differential cell adhesion on mesoporous silicon substrates, *ACS Appl Mater Interfaces* **2012**, *4,* 2903–2911.

(13) Esumi K., Hosoya T., Suzuki A. and Torigoe K. Formation of Gold and Silver Nanoparticles in Aqueous Solution of Sugar-Persubstituted Poly(amidoamine) Dendrimers. *J Coll and Interf Sc* **2000,** *226*, 346–352.

(14) Ismail I.M., Ewais H.A. Mechanistic and kinetic study of the formation of silver nanoparticles by reduction of silver(I) in the presence of surfactants and macromolecules. *Transition Met Chem* **2015,** *40*, 371–378.

(15) Patakfalvi R., Papp S. and Dékany I. The kinetics of homogeneous nucleation of silver nanoparticles stabilized by polymers, *J Nanopar Res* **2007**, *9*, 353–364.

(16) Pacławski K. and Sak T. Kinetics and mechanism of the reaction of gold(iii) chloride complexes with formic acid, *J Min Metall Sec. B-Metall* **2015**, *51 (2) B*, 133-142.

(17) Mohammadnejad S., Provis J. L., Van Deventer J. S. J. Reduction of gold(III) chloride to gold(0) on silicate surfaces, *J Colloid Interf Sci* **2013**, *389*, 252–259

(18) Abdelhalim M.A.K., Mady M.M., Ghannam M.M. Physical Properties of Different Gold Nanoparticles: Ultraviolet-Visible and Fluorescence Measurements. *J Nanomed Nanotechol* **2012**, *3*, 133

(19) Evanoff D.D., Chumanov G. Size-Controlled Synthesis of Nanoparticles. 2. Measurement of Extinction, Scattering, and Absorption Cross Sections *J Phys Chem B*. **2004**, *108* (37), 13957-13962.

(20) Demers Steven M. E., Hsieh Lee J. H., Shirazinejad Cyna R., Garcia John Luke A., Matthews James R., and Hafner Jason H. Ultraviolet Analysis of Gold Nanorod and Nanosphere Solutions *J Phys Chem C* **2017**,*121(9)* 5201-5207

(21) Gentile F., Battista E., Accardo A., Coluccio M.L., Asande M., et al. Fractal structure can explain the increased hydrophobicity of nanoporous silicon films. *Microelectron Eng* **2011**, *88*, 2537–2540.

(22) Marinaro G., La Rocca R., Toma A., Barberio M., Cancedda L., et al. Networks of neuroblastoma cells on porous silicon substrates reveal a small world topology. *Integr Biol* **2015,** *7,* 184–197.

(23) Gentile F., Coluccio M.L., Toma A., Rondanina E., Leoncini M., et al. Electroless deposition dynamics of silver nanoparticles clusters: a diffusion limited aggregation (DLA) approach, *Microelectron Eng* **2012**, *98*, 359–362.

(24) Meakin P. Diffusion-controlled deposition on surfaces: Cluster-size distribution, interface exponents, and other properties *Phys. Rev. B: Condens Matter Mater Phys* **1984,** *30*, 4207–4214.

(25) Enustun B. V. and Turkevich J. Coagulation of Colloidal Gold *J Am Chem Soc* **1963**, *85*, 3317-3328.

(26) Polte Jörg Fundamental growth principles of colloidal metal nanoparticles – a new perspective *Cryst Eng Comm* **2015**, *17*, 6809–6830.

(27) Simonin J.P. On the comparison of pseudo-first order and pseudo-second order rate laws in the modeling of adsorption kinetics *Chem Eng J* **2016**, *300*, 254–263.

(28) Mie, G. Beiträge zur Optik trüber Medien, speziell kolloidaler Metalllösungen. *Ann Phys* **1908**, *25*, 377–445.

(29) Karg M., König Tobias A.F., Retsch M., Stelling C., Reichstein Paul M., Honold T., Thelakkat M. and Fery A. Colloidal self-assembly concepts for light management in photovoltaics, *Mater Today* **2015,** *18* (4), 185-205.

FIGURE CAPTIONS

Figure 1. Gold nanospheres production by porous silicon nanoparticles oxidation.

Figure 2. SEM images of gold nanoparticles acquired after 120 min of reaction at temperature of 50°C, corresponding to the final steady state of the process (see results section).

Figure 3. Absorbance (Abs) spectra of the gold nanoparticles solutions at different times of reaction for temperature T_1 (20°C) and T_2 (50°C).

Figure 4. Absorbance versus time plots for the gold nanoparticles solutions for temperature T_1 and T_2 on at 560 nm. *Upper line* range 0-300 min, *lower line* range 0-3000 min.

Figure 5. Plots of ln(a/(1-a) vs time for T_1 and T_2, experimental data (points) and fitting (continuous lines).

Figure 6. Plots of gold absorbance band vs time for T_1 and T_2, experimental data (points) and fitting (continuous lines).

Figure 7. SEM micrographs of gold nanoparticles in two experiments (T_1 and T_2) and two step time points for both temperatures.

Figure 8. Numerical DLA aggregates as a function of the radius R of the circle of nucleation sites (a). Time evolution of the aggregate for $R = 30$ pixels (b). Time evolution of the aggregates for $R = 10, 20, 30, 40$ pixels (c). Time evolution of the density ρ of the aggregates (d). Normalized density ρ of the aggregates as a function of R (e). Density-density correlation function of the aggregates, with a typical scaling law behavior.

Table 1. Observed rate constants (k_{obs}) for the gold/Si reactions at T_1=20°C and T_2=50°C, determined from the slopes of the linear fit to the plots ln(a/(1-a)) vs time in the range 0-120 min.

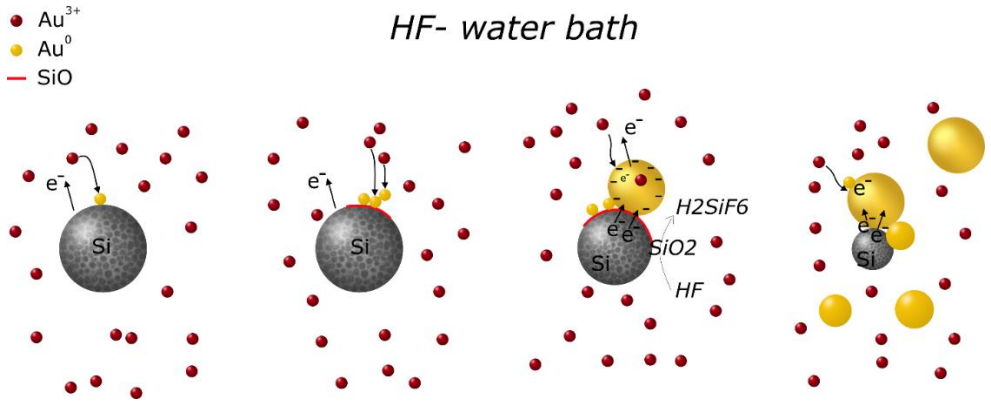

Figure 1

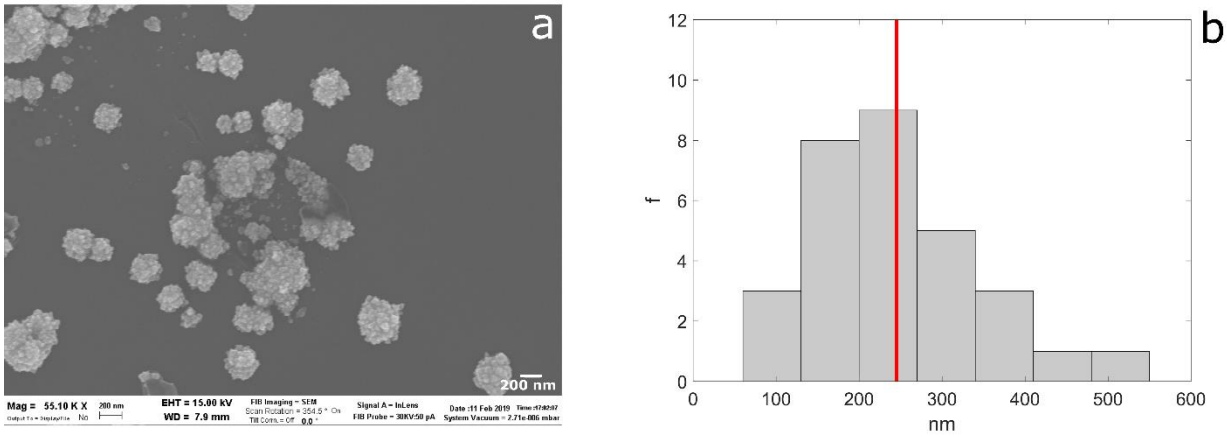

Figure 2

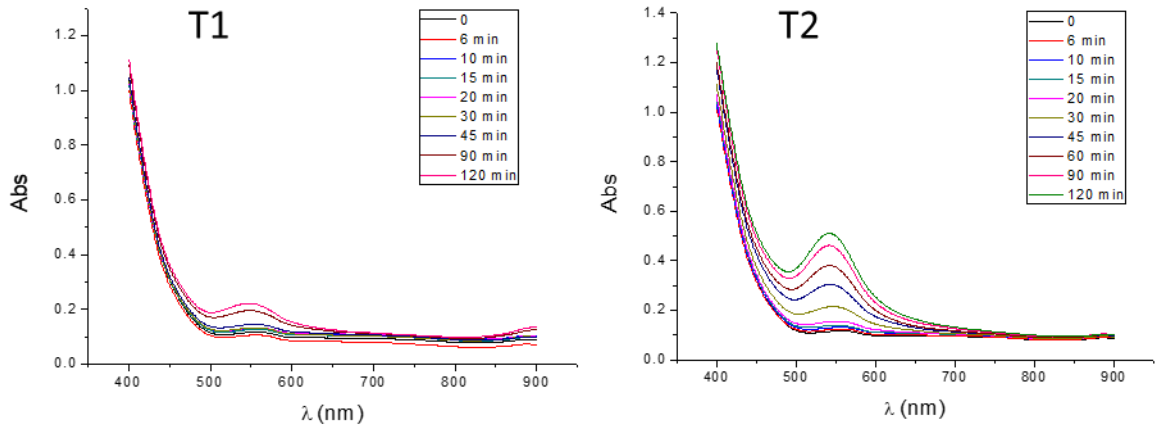

Figure 3

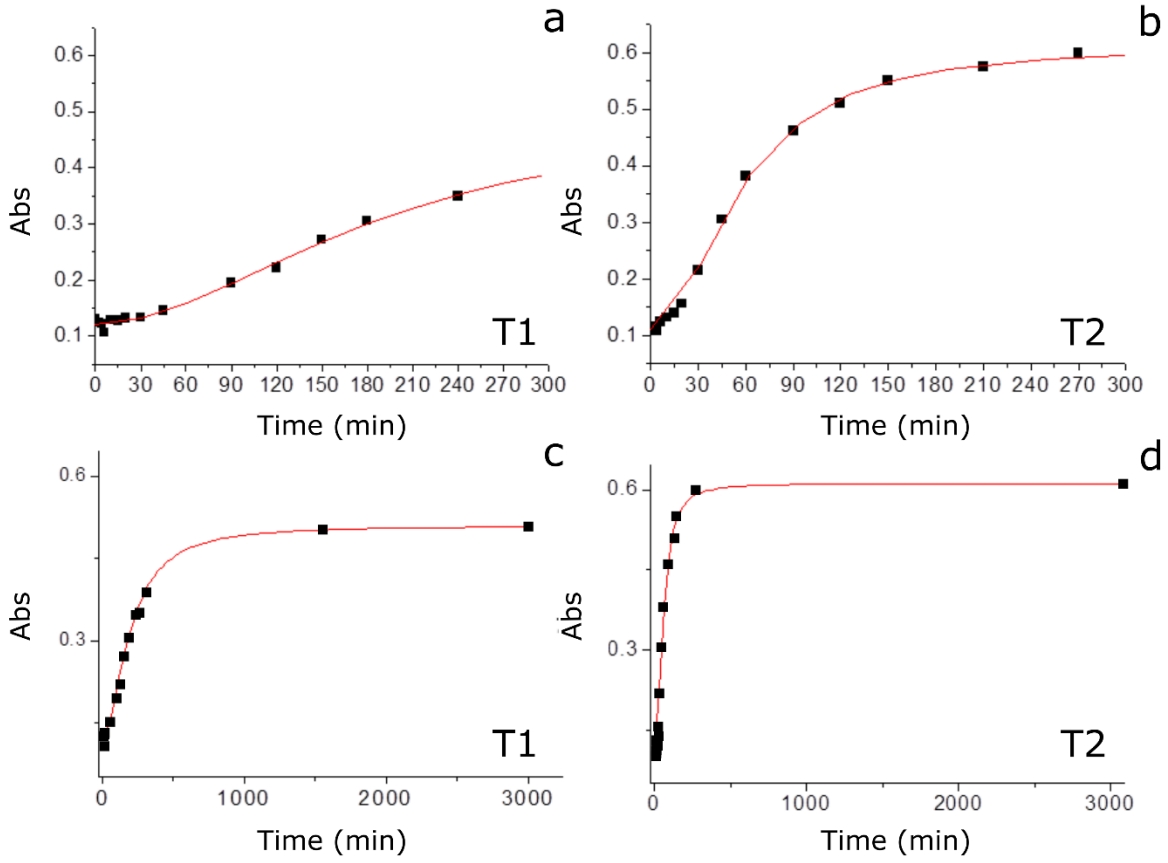

Figure 4

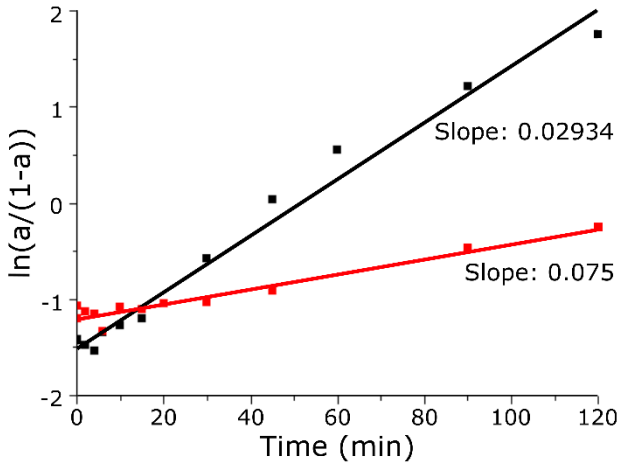

Figure 5

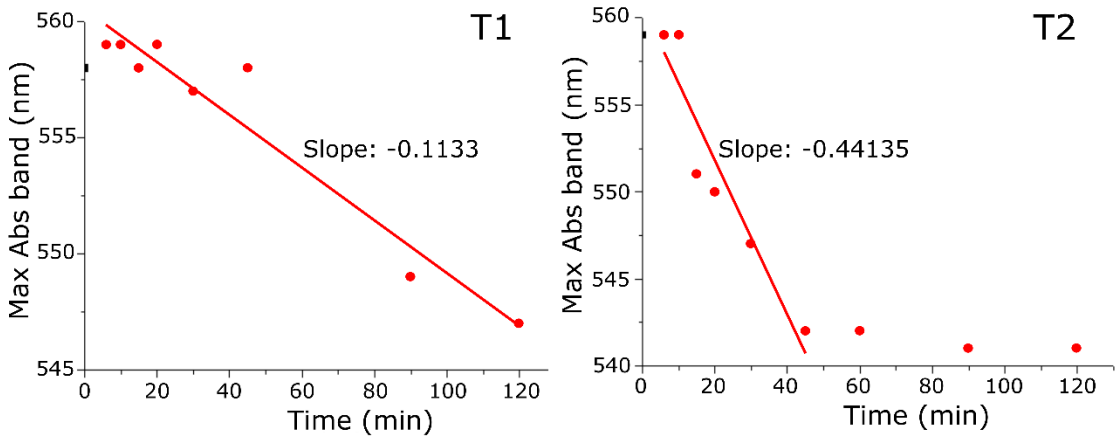

Figure 6

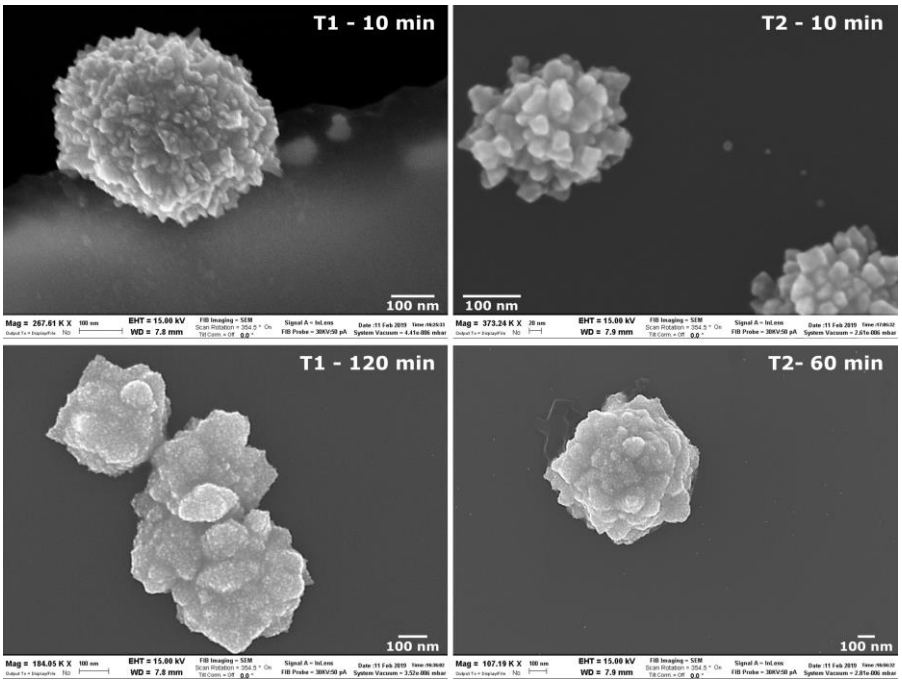

Figure 7

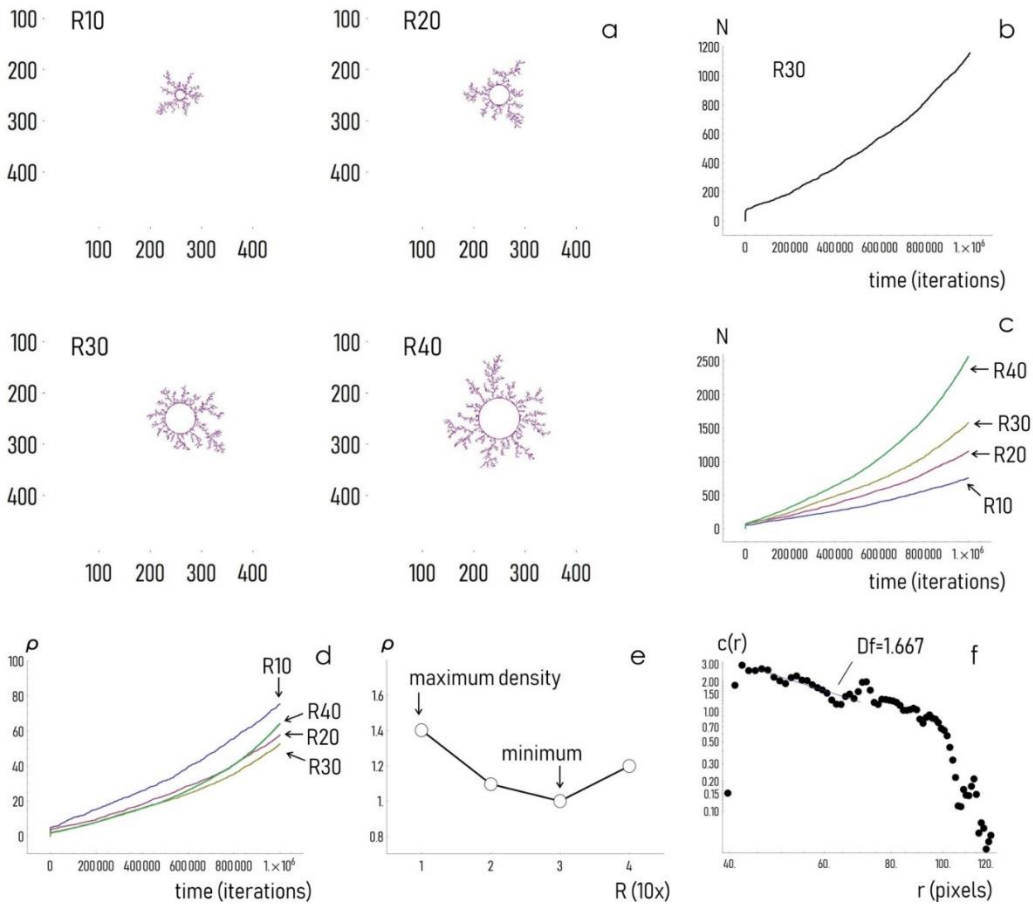

Figure 8

Temperature °C	k_{obs}
20	$7 \cdot 10^{-3}$ s^{-1}
50	$2.9 \cdot 10^{-2}$ s^{-1}

Table 1